AD-A194 611 MEASUREMENTS OF XEF (XENON FLUORIDE) GROUND STATE DISSOCIATION AND VIBRAT (U) AEROSPACE CORP EL SEGUNDO CA AEROPHYSICS LAB J F BOTT ET AL 25 MAR 88 TR-0088(3930-04)-1 SD-TR-88-54

1/1

UNCLASSIFIED

F/G 7/2

NL

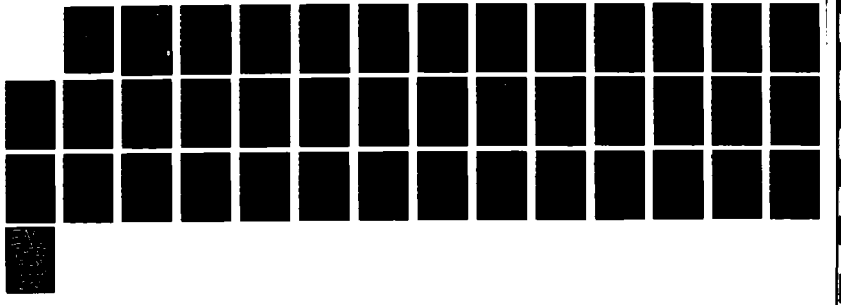

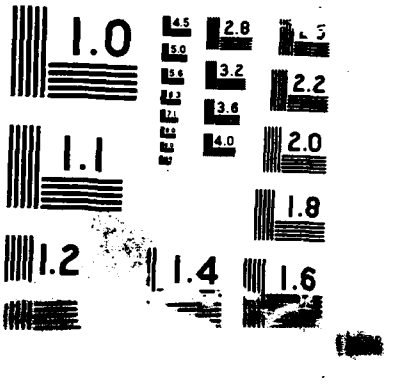
1.0
1.1
1.2
1.4
1.6
1.8
2.0
2.2
2.8
3.2
3.6
4.0
4.5
5.0

REPORT SD-TR-88-54

Measurements of XeF Ground State Dissociation and Vibrational Equilibration

J. F. BOTT, R. F. HEIDNER, J. S. HOLLOWAY
J. B. KOFFEND, and M. A. KWOK
Aerophysics Laboratory
Laboratory Operations
The Aerospace Corporation
El Segundo, CA 90245

25 March 1988

Prepared for

SPACE DIVISION
AIR FORCE SYSTEMS COMMAND
Los Angeles Air Force Base
P.O. Box 92960, Worldway Postal Center
Los Angeles, CA 90009-2960

This report was submitted by The Aerospace Corporation, El Segundo, CA 90245, under Contract No. F04701-85-C-0086-P00019 with the Space Division, P. O. Box 92960, Worldway Postal Center, Los Angeles, CA 90009. It was reviewed and approved for The Aerospace Corporation by W. P. Thompson, Director, Aerophysics Laboratory. Lt. Scott W. Levinson/SD/CNW was the project officer for the Mission-Oriented Investigation and Experimentation (MOIE) Program.

This report has been reviewed by the Public Affairs Office (PAS) and is releasable to the National Technical Information Service (NTIS). At NTIS, it will be available to the general public, including foreign nationals.

This technical report has been reviewed and is approved for publication. Publication of this report does not constitute Air Force approval of the report's findings or conclusions. It is published only for the exchange and stimulation of ideas.

SCOTT W. LEVINSON, Lt, USAF
MOIE Project Officer
SD/CNW

RAYMOND M. LEONG, Major, USAF
Deputy Director, AFSTC West Coast Office
AFSTC/WCO OL-AB

UNCLASSIFIED

SECURITY CLASSIFICATION OF THIS PAGE

REPORT DOCUMENTATION PAGE

1a. REPORT SECURITY CLASSIFICATION Unclassified	1b. RESTRICTIVE MARKINGS
2a. SECURITY CLASSIFICATION AUTHORITY	3. DISTRIBUTION / AVAILABILITY OF REPORT Approved for public release; distribution unlimited.
2b. DECLASSIFICATION / DOWNGRADING SCHEDULE	
4. PERFORMING ORGANIZATION REPORT NUMBER(S) TR-0088(3930-04)-1	5. MONITORING ORGANIZATION REPORT NUMBER(S) SD-TR-88-54
6a. NAME OF PERFORMING ORGANIZATION The Aerospace Corporation Laboratory Operations 6b. OFFICE SYMBOL (If applicable)	7a. NAME OF MONITORING ORGANIZATION Space Division
6c. ADDRESS (City, State, and ZIP Code) El Segundo, CA 90245	7b. ADDRESS (City, State, and ZIP Code) Los Angeles Air Force Base Los Angeles, CA 90009-2960
8a. NAME OF FUNDING / SPONSORING ORGANIZATION 8b. OFFICE SYMBOL (If applicable)	9. PROCUREMENT INSTRUMENT IDENTIFICATION NUMBER F04701-85-C-0086-P00019
8c. ADDRESS (City, State, and ZIP Code)	10. SOURCE OF FUNDING NUMBERS PROGRAM ELEMENT NO. / PROJECT NO. / TASK NO. / WORK UNIT ACCESSION NO.

11. TITLE (Include Security Classification)
Measurements of XeF Ground State Dissociation and Vibrational Equilibration

12. PERSONAL AUTHOR(S)
Bott, J. F., Heidner, R. F., Holloway, J. S., Koffend, J. B., and Kwok, M. A.

13a. TYPE OF REPORT	13b. TIME COVERED FROM ____ TO ____	14. DATE OF REPORT (Year, Month, Day)	15. PAGE COUNT
		1988 March 25	41

16. SUPPLEMENTARY NOTATION

17. COSATI CODES			18. SUBJECT TERMS (Continue on reverse if necessary and identify by block number)
FIELD	GROUP	SUB-GROUP	Excimer lasers; XeF (xenon fluoride); Chemical lasers; XeF_2 (xenon difluoride)

continued

19. ABSTRACT (Continue on reverse if necessary and identify by block number)

The removal rates of the lower levels of the laser transitions affect the efficiency of the XeF excimer laser performance. We have deduced the removal rates of XeF(X,v) in argon, helium, and neon by measuring the populations of v = 0 and 1 vibrational levels formed by the photolysis of XeF_2. The time history of each vibrational population is monitored with a cw tunable dye laser tuned to an absorption feature of the selected vibrational/rotational level. The studies show a rapid vibrational relaxation of v = 0 and v = 1 levels followed by a common decay rate of the two levels. Helium and neon were found to remove these levels with the same rate coefficient of $(2.0 \pm 0.2) \times 10^4$ $(sec\text{-}Torr)^{-1}$ at room temperature. The rate coefficients for argon were faster by about 25%. The removal rate coefficients increased with temperature in the range of 23 to 95°C. The vibrational relaxation rate coefficient for the excitation of v = 1 from v = 0 by helium was measured to be $(3.6 \pm 0.7) \times 10^5$ $(sec\text{-}Torr)^{-1}$ at room temperature. This is considerably faster than the rate of $(4.8 \pm 1.5) \times 10^4$ $(sec\text{-}Torr)^{-1}$ previously reported by Fulghum et al. It should be possible

20. DISTRIBUTION / AVAILABILITY OF ABSTRACT	21. ABSTRACT SECURITY CLASSIFICATION
☒ UNCLASSIFIED/UNLIMITED ☐ SAME AS RPT ☐ DTIC USERS	Unclassified
22a. NAME OF RESPONSIBLE INDIVIDUAL	22b. TELEPHONE (Include Area Code) / 22c. OFFICE SYMBOL

DD FORM 1473, 84 MAR 83 APR edition may be used until exhausted. All other editions are obsolete.

SECURITY CLASSIFICATION OF THIS PAGE

UNCLASSIFIED

to extend the present methods to the higher vibrational levels of v = 2-4 which are of particular importance to the laser operation.

Preliminary measurements of the absorption spectra of XeF(X,v=1,2) have been recorded. The spectra for v = 1 are in good agreement with simulated spectra based on literature values of the spectral constants. However, the agreement for the v = 2 spectra is not so good. Such measurements with the high-resolution tunable dye laser probe offer the possibility of refining the spectral constants as well as measuring pressure-broadening coefficients.

The absorption coefficient of XeF_2 has been measured at 193, 206, and 253 nm. We have determined experimentally that the absorption of 1 photon at 193 nm leads to the dissociation of 1 XeF_2 molecule.

Block 18 (continued): Vibrational relaxation
Molecular dissociation
Spectroscopy

PREFACE

This report reflects research supported by the Air Force Weapons Laboratory of the Department of Defense under U. S. Air Force Space Division Contract F04701-85-C-0086. Acknowledgment is made to Dr. L. E. Wilson, Air Force Weapons Laboratory, for his continuing interest in this work.

CONTENTS

TABLES

FIGURES

FIGURES (continued)

I. INTRODUCTION

Performance calculations for E-beam pumped, high pressure XeF lasers require rate coefficients for the kinetic processes responsible for the production and removal of the several electronic-vibronic states of XeF. In particular, the intrinsic efficiency of the XeF laser depends directly on processes such as molecular dissociation and vibrational relaxation which empty the lower levels of the laser transitions. The XeF molecule in the ground electronic state is dissociated rapidly by collision processes at room temperature because of its shallow well depth. Its 1175 cm^{-1} well depth[1] only allows for about nine vibrational levels below the dissociation limit. Rapid dissociation of the ground state at a pressure of a few atmospheres keeps the lower levels of the laser transition from filling up and shutting off the laser action. Rapid vibrational relaxation also helps to spread the population over several vibrational levels.

Fulghum, Feld, and Javan[2,3,4] have previously performed a room-temperature study of XeF ground state kinetics for vibrational levels v = 0 and 1. They could not measure separate state-to-state rate coefficients for dissociation and vibrational relaxation, but they did deduce them from model calculations fitted to their experimental data. Although the model calculations are based on room temperature data for v = 0 and 1, the laser operates best at elevated temperatures, and the laser transitions terminate on vibrational levels v = 2-4. Therefore, present laser model predictions depend on extrapolations of the Fulghum rate coefficient model to the required temperature and vibrational levels. These extrapolations are uncertain because so little is known about dissociation and vibrational relaxation processes in such shallow-well molecules.

The studies of Fulghum et al. were very important in providing preliminary values of these rate coefficients. The method of studying the ground state processes can be improved, however, with new, commercially available, cw tunable dye lasers and with a different digital acquisition technique. The present effort is directed toward measuring the temperature-dependent rate coefficients for the coupled relaxation and dissociation of the ground state of XeF for the important vibrational levels of v = 2-4. However, in this interim report, we will describe the apparatus and present the results of

II. EXPERIMENTAL METHOD AND APPARATUS

A convenient method of obtaining ground state XeF is the UV photolysis of XeF_2 with a 15-nsec ArF excimer laser pulse at 193 nm. The photolysis can produce XeF(X,v) directly, or electronically excited XeF(B) which decays with a 14-nsec lifetime[6] to the ground electronic state, XeF(X,v). This technique was used by Fulghum et al.[3,4] and in the present study. However, we use a different method of monitoring the XeF(X,v). Fulghum used a pulsed, tunable dye laser to pump a small fraction of the XeF(X,v=0,1) to the B state and recorded the subsequent B-state fluorescence with a boxcar integrator as a function of the delay time between the dye laser and the photolysis laser. Using this method, the time history of the XeF(X,v=0) or XeF(X,v=1) population could be determined.

Our method is to monitor selected vibrational levels of the ground state with a frequency-doubled cw ring dye laser tuned to absorption features near 350 nm. See Fig. 1 for a schematic representation of the potential diagram of XeF. The tunable dye laser passes through the cell containing the photolysis-produced XeF(X) and is monitored with a photomultiplier whose signal is recorded with a transient digitizer and then averaged. The absorption of this dye laser beam depends directly on the concentration of the selected vibrational level of XeF. Therefore, the removal rate of that level by dissociation and vibrational relaxation can be determined from the time behavior of the transmitted signal. The advantage of this technique is that the whole time profile can be recorded for each ArF laser pulse so that the resulting signal-averaged profile has a better signal/noise ratio for the same number of ArF laser shots. An attempt was made to use the B-state fluorescence induced by the cw dye laser as a measure of the ground-state population. However, the emission from the initial B-state population produced by the ArF laser pulse was found to swamp the laser-induced fluorescence. Even the use of a KrF laser as the photolysis laser produced too much initial B-state emission. Helm et al.[7] have described observations of B-state emission from KrF photolyzed mixtures containing XeF_2. Fulghum overcame this problem with the use of the pulsed dye laser, which has a much larger peak power than the cw dye laser, so that the laser-induced fluorescence signal was much greater than that of the photolysis background.

A schematic of the apparatus is shown in Fig. 2. The main elements include the Lambda Physik excimer laser (ArF), a flow cell and gas handling system, a Coherent Radiation 699-21 frequency-doubled cw tunable ring dye laser, a Burleigh wavemeter, a McPherson monochromator, a photomultiplier, a Transiac transient recorder, and a DEC 11/23 computer for data acquisition and storage.

Room temperature measurements were made in a 5-cm-dia flowtube made of stainless steel and two sections of anodized aluminum. It is more accurately described as an absorption cell through which gas flows slowly to replenish the photolyzed XeF_2. The stainless steel was coated with Teflon to reduce the loss of XeF_2 to the walls. Suprasil windows mounted in aluminum and brass window holders define the length of the cell to be 75 cm. A mixing vessel made of stainless steel holds the XeF_2 crystals and can be cooled to control the vapor pressure of the XeF_2, which is about 4.4 Torr at 298 K (Ref. 8). A diluent such as argon can be flowed through the mixing vessel to carry the XeF_2 into the absorption cell where it can be diluted further with another stream of argon or other collision partner. This allows the total pressure of the argon to be varied independently of the partial pressure of the XeF_2. Experiments were performed in which the absorption by the XeF_2 at 206 nm was monitored at different pressure/flow settings. The pressures and flow rate settings were calculated and adjusted to maintain a constant density of XeF_2. The calculated and measured densities of XeF_2 correlated within an experimental error of about ±3%. Flow velocities of 2.5 to 5 cm/sec are controlled by a throttle valve just downstream of the flowtube. These velocities allow replacement of the photolyzed XeF_2 without wasting it. Baratron gauges are used to measure the pressures in the flowtube and in the XeF_2 reservoir. The temperature of the absorption cell is measured with a thermocouple.

A second flowtube designed for studies at elevated temperatures is a straight copper tube with window flanges on the ends and inlet and outlet ports for the gas flow. Thermocouples are located at the two ends and in the middle of the flowtube. The copper tube is wrapped with heating tape and insulation to permit elevated-temperature studies. The distance between the windows is 59.7 cm, although extensions to the tube permit heating outside the windows to ensure a uniform temperature in the flowtube.

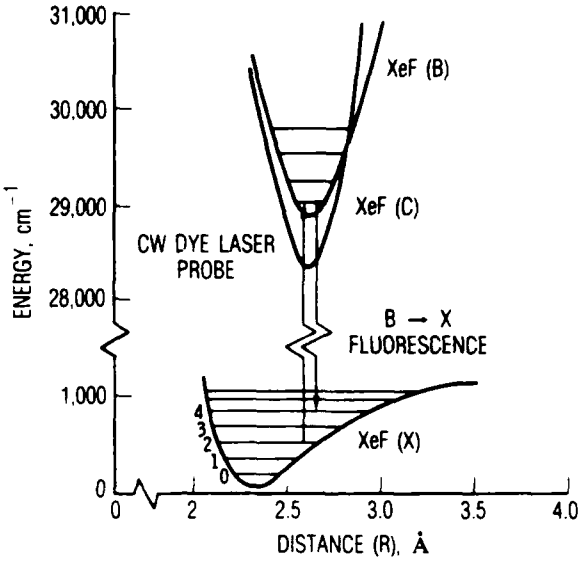

Fig. 1. Potential Energy Diagram of XeF.

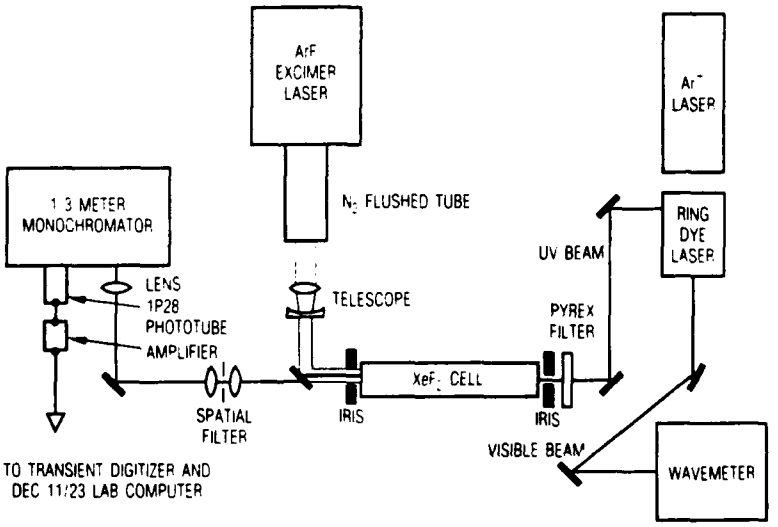

Fig. 2. Schematic of apparatus.

The Lambda Physik excimer laser produces 15-nsec pulses with energies of about 140 mJ when lasing on ArF at 193 nm. However, atmospheric absorption and losses in the optical train attenuate the energy by about a factor of 2 even though the path is partly flushed with nitrogen. The beam is compressed by a factor of 2 with a telescope and turned 90 deg with a front-surface dielectric mirror. An 8-mm-dia aperture cuts off some of the 12-mm-dia photolysis beam, but the remaining beam is sufficiently large for the 2-mm-dia probe beam. The purpose of the aperture is to produce a more uniform photolysis beam and to decrease the amount of XeF_2 photolyzed by each pulse. Too small an aperture was found to produce steering of the tunable dye laser beam; otherwise an even smaller aperture would have been used. The energy fluence of the pulse entering the flow cell is about 0.1 J/cm^2.

The dye laser is pumped by a Coherent Radiation Ar^+ ion laser (Innova 100) operating multiline at a power level of 7.5 W. Operating on DCM Special dye, the doubled dye laser has a power of ~ 0.1 mW at wavelengths between 320 and 345 nm, with a bandwidth of about 2 MHz. Its wavelength (before doubling) is monitored with a Burleigh wavemeter Model WA-20 with an accuracy of 0.001 nm; this translates to an accuracy of 0.0005 nm near 350 nm for the doubled dye laser. At 25°C the Doppler width of each vibronic line is about 0.00032 nm, which is slightly smaller than the resolution of the wavemeter. A calculation[9] of the absorption spectrum with the resolution of the Doppler width (pressure-broadening should be small at pressures less than 100 Torr) shows the picket fence nature of the absorption features, with line spacings typically 0.002 to 0.004 nm. The wavemeter allows relatively unambiguous line identification, at least for v = 0 and 1 vibrational levels. However, the final adjustment of the tunable dye laser is made on the basis of the observed signal. The 2-mm-dia probe beam is attenuated by a factor of 100 before it enters the flow cell to prevent any slow but steady photolysis of the XeF_2 or any bleaching of the XeF(X,v) absorption feature. Careful alignment of the probe beam and the ArF laser photolysis beam is required to maximize the signal and to minimize beam steering effects.

An RCA 1P28 photomultiplier mounted on the exit slit of a McPherson 218 1/3 m monochromator is used to monitor the intensity of the probe beam after it exits the flow cell. The monochromator was placed 2 m from the cell to discriminate against the initial B-state emission produced by the photo-

lysis. A Pacific Instruments Model 2A50 video amplifier (×100) mounted directly on the photomultiplier amplifies the signals to the range required by the Transiac transient recorder. The amplifier has an input impedance of 50 ohms; it is terminated with a 50-ohm resistor and ac coupled to the Transiac transient recorder. The photomultiplier is operated at a low voltage of 500 V to prevent both high dc anode currents and any saturation of the amplifier. There is a careful balance in the design of the detection system to optimize the signal/noise ratio without saturating the several components of the system with the dc signal of the tunable dye laser. The output of the transient recorder is stored in the DEC 11/23 for signal averaging. The response time of the detection system is limited by the 10- to 12-nsec rise time of the amplifier/photomultiplier and the 10-nsec bin size of the Transiac recorder. These times are comparable to the ArF laser pulse width of 15 nsec.

III. EXPERIMENTAL RESULTS

A. SPECTRAL SCANS OF XeF(X)

Scans of the absorption spectrum of XeF(X,v) were recorded to find appropriate absorption features for the kinetic measurements. With a slow flow of XeF_2 throttled to give a pressure of about 0.75 Torr in the cell and the ArF laser operating at 10 Hz, the photolyzed gas was probed with the tunable dye laser operating in the scan mode. The tunable dye laser was monitored, with the photomultiplier output being sent directly to two channels of a Stanford Research Systems Model SR 250 boxcar averager. The gate for one channel was set to record the signal before the pulsed photolysis laser; the gate for the second channel was placed 200 nsec after the photolysis laser pulse and the formation of XeF. The ratio of these two signals should not be affected by the slow changes in the intensity of the dye laser as it scans over its spectral range. A sample of the data obtained for the v" = 1 to v' = 1 transitions near 345 nm (28950 cm^{-1}) is shown in Fig. 3. Koffend has written a spectrum synthesis code[9] for band identification. A spectrum generated with this code and the spectroscopic data of Tellinghuisen et al.[1] is shown in Fig. 4 for the same spectral range as the measured spectrum of Fig. 3. The synthetic spectrum was generated for a bandwidth of 1.6 GHz (0.0006 nm), including all the isotopes (there are four major ones) of xenon. Although the bandwidth is about twice the calculated value for a Doppler-broadened line, the agreement is excellent. Measurements of the v" = 2 to v' = 2 bands are not in as good agreement with the simulations and are still being studied. Scans have also been obtained for the v" = 2 to v' = 0 transitions (some of the features may also be v" = 4 to v' = 1 transitions) and for the v" = 3 to v' = 0 bands. These latter measurements were obtained with a Kr ion laser pumping Rhodamine 700 dye.

B. ABSORPTION BY XeF_2

Experiments were performed to determine the spectral absorption coefficients of XeF_2 at 193 nm, the wavelength of the ArF laser, and also at 253 nm. The ArF laser, apertured to a 1-mm diameter without the telescope and attenuated a factor of 300 by neutral density filters, was monitored with Si photodiodes before and after passing through the absorption cell. Beam

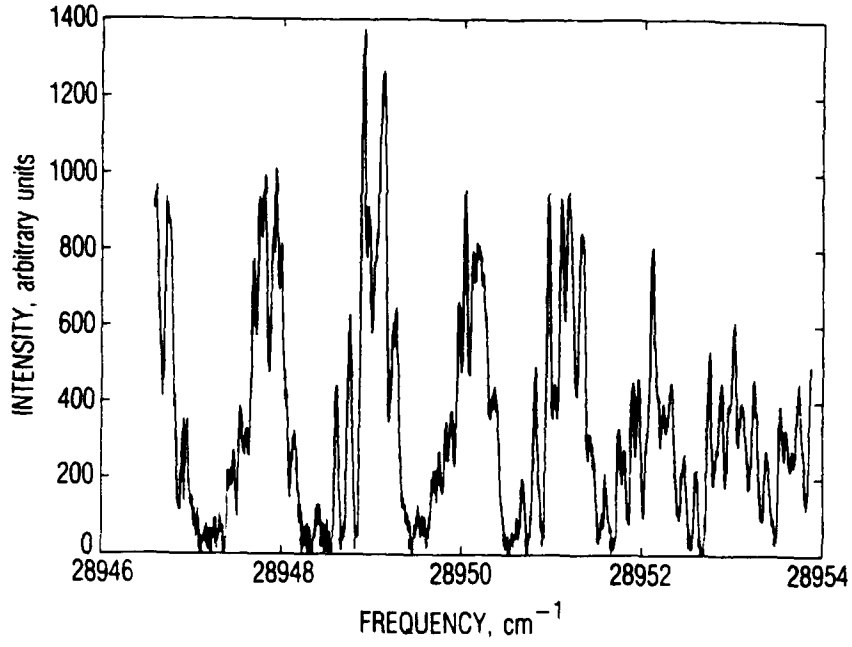

Fig. 3. Spectral scan in v" = 1 to v' = 1 band of XeF(X).

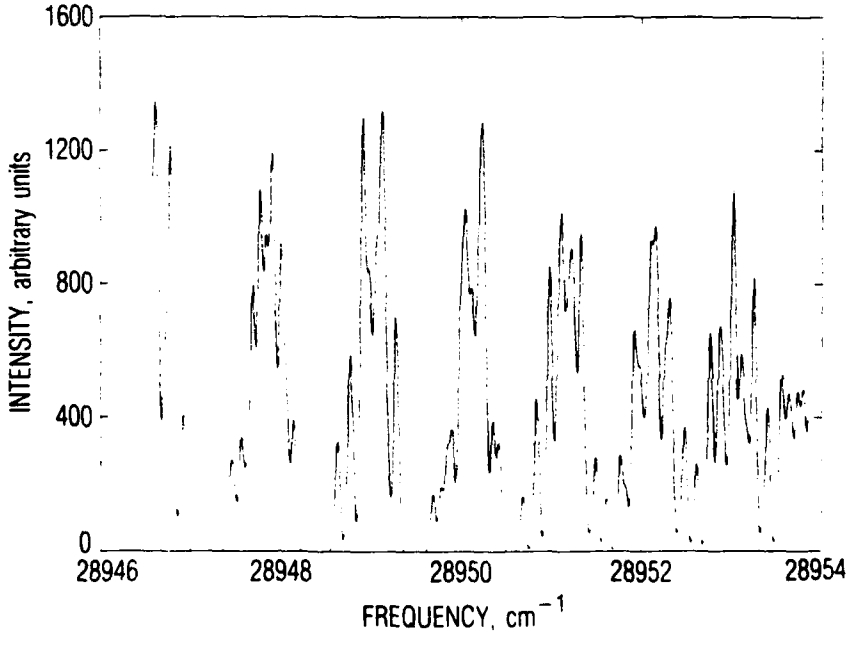

Fig. 4. Simulation of the v" = 1 to v' = 1 band of XeF(X).

splitters reflected a fraction of the beam to the photodiodes to avoid their saturation. A collimated beam from a deuterium lamp was passed in the opposite direction, filtered with a Hg line UV interference filter, and monitored with a photomultiplier. The data could be recorded simultaneously to improve the accuracy of the absorption coefficients relative to each other. Measurements were recorded for XeF_2 pressures between 0.143 and 1.24 Torr, and the data are shown in Fig. 5. From these data and a cell length of 75 cm, we calculate an absorption coefficient at 193 nm of 1.963/75 = 0.0262 $(Torr\text{-}cm)^{-1}$ or 7.9×10^{-19} cm^2 for the cross section. We obtained a value of 8.0×10^{-20} cm^2 for the cross-section at 253 nm.

We measured the absorption coefficient of XeF_2 at 206 nm in a separate experiment in the 59.7-cm copper flowtube. A deuterium lamp filtered with a 206-nm interference filter was passed through the flowtube to the McPherson monochromator and photomultiplier. With the flowtube initially evacuated and the XeF_2 reservoir pumped down to its vapor pressure, a low-pressure flow through the flowtube was established. Both the pressure in the flowtube and the photomultiplier signal were recorded with the computer with a 12-bit A to D converter. Once the throttle valve was shut, the pressure rose to 1.4 Torr in about 1 min. Figure 6 shows the natural logarithm of the transmission plotted versus the pressure (reduced to XeF_2 number density for the temperature of 21°C). From the slope of the data and the 59.7-cm length of the cell, we calculate an absorption coefficient of 2.56×10^{-19} cm^2. These measurements were repeated with the flowtube heated to 81°C, and a somewhat larger value of 2.96×10^{-19} cm^2 was obtained from the data of Fig. 7.

In Ref. 10 Black et al. plotted absorption coefficients of XeF_2 which have been measured between 140 and 280 nm by themselves and two other groups. Measurements between 170 and 210 nm by Black et al. overlap measurements between 203 and 280 nm reported by Jortner et al.[11] but disagree by a factor of 2.4 in the region of overlap. Our measurement of 0.0262 $(Torr\text{-}cm)^{-1}$ or 7.9×10^{-19} cm^2 at 193 nm is approximately 32% higher than the value of 6.0×10^{-19} cm^2 shown by Black et al. Likewise, our value of 2.56×10^{-20} cm^2 at 206 nm is 34% larger than the value of 1.87×10^{-19} cm^2 reported by Black et al. On the other hand, our value of 8.0×10^{-20} cm^2 at 253 nm is less than the value of 1.6×10^{-19} cm^2 reported by Jortner et al.[11]. When both sets of data shown in Ref. 10 are scaled to agree with our three data points, they

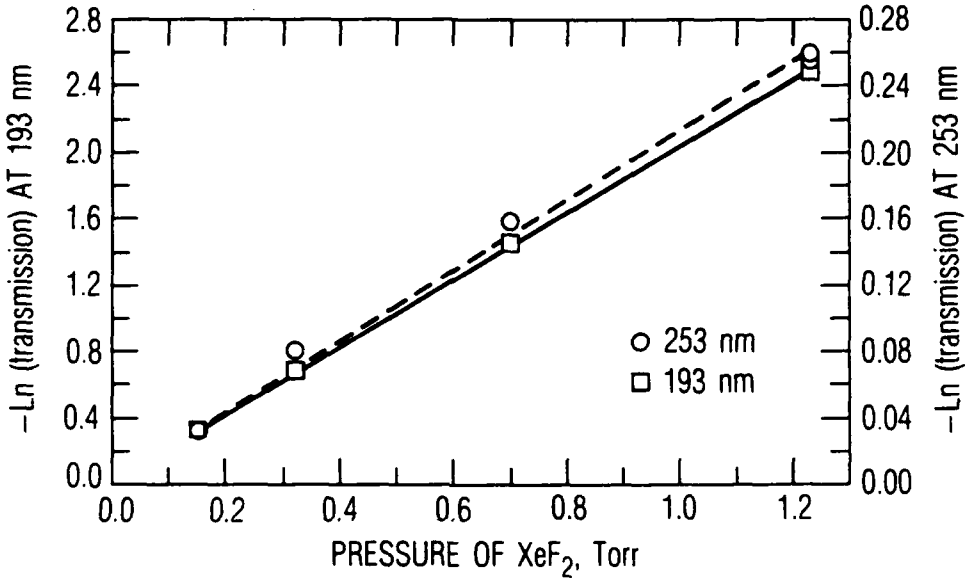

Fig. 5. Plot of XeF_2 absorption, -ln(transmission) versus XeF_2 pressure. Squares = data for 193 nm. Circles = data for 253 nm.

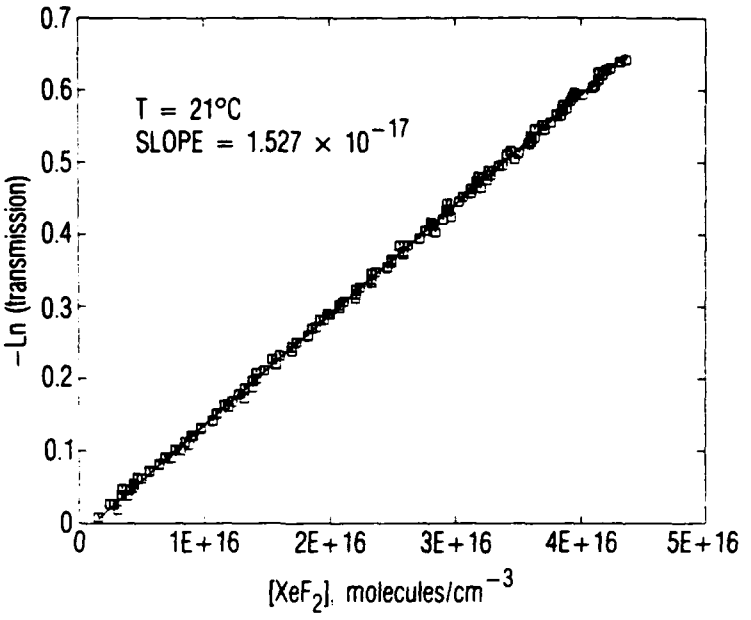

Fig. 6. Plot of XeF_2 absorption at 206 nm, -ln(transmission) versus XeF_2 density. Temperature = 21°C.

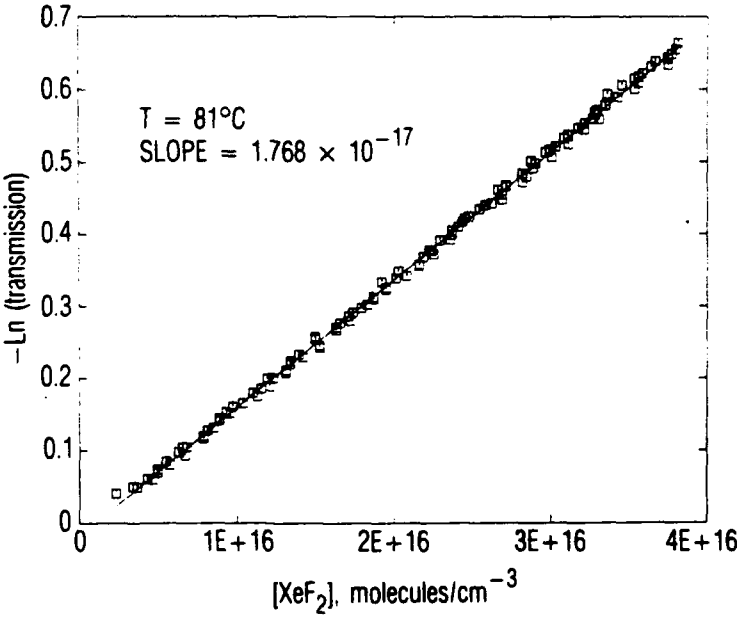

Fig. 7. Plot of XeF_2 absorption at 206 nm, -ln(transmission) versus XeF_2 density. Temperature = 81°C.

agree in the region of overlap. This would suggest that the difficulty of measuring the partial pressure of XeF_2 accounts for the systematic source of the discrepancy in the previously reported data.

We found that when XeF_2 was isolated in the copper flowtube for 8 min, the absorption decrease indicated a change of 5% or less in the XeF_2 density. In contrast, the XeF_2 had a lifetime of about 12 to 15 min in the Teflon-coated stainless steel and aluminum flowtube.

Both the absorption coefficient and the quantum yield of the photolysis products are of importance in designing an experiment based on the photolysis of XeF_2. We have measured the quantum yield of dissociation products per photon absorbed in the following way. The copper flowtube was filled with XeF_2 to a pressure of 1.34 Torr and isolated with the valves. The pressure in the flowtube was monitored with the Baratron gauge, while the ArF laser was used to photolyze the XeF_2. The energy of the photolysis pulses was monitored with a Laser Precision energy meter; it was calibrated in situ and recorded a measured fraction of the total pulse energy before it entered the cell. The energy/pulse is plotted versus time in Fig. 8 for two sequences. Note the break in the laser power and its slow recovery. A certain fraction of the laser pulse is absorbed by the XeF_2 in accordance with the partial pressure of XeF_2 and its cross section at 193 nm. We have modeled this photolysis sequence using our measured cross section of 7.9×10^{-19} cm^2 and the assumption that the absorption of one photon results in the removal of 1 XeF_2 molecule, leading ultimately to the formation of 1 Xe and 1 F_2. The immediate photolysis product of XeF(B) radiates to the ground state which collisionally dissociates to Xe + F. The F atoms recombine on the walls to form F_2. The consequence of these processes is that two molecules are produced for each molecule dissociated, with an accompanying increase in pressure. Our calculated pressure profile for the laser sequence in Fig. 8 is shown in Fig. 9 along with the measured pressure history. The excellent agreement justifies the assumption of the 100% photolysis yield.

C. RATES OF XeF(X,v=0) VIBRATIONAL RELAXATION AND REMOVAL

For measurements of the removal rates of XeF(X,v=0), we chose an absorption feature in the 0 → 5 band near a nominal wavelength of 329.563 nm as indicated by the wavemeter. The amplified photomultiplier signal was recorded

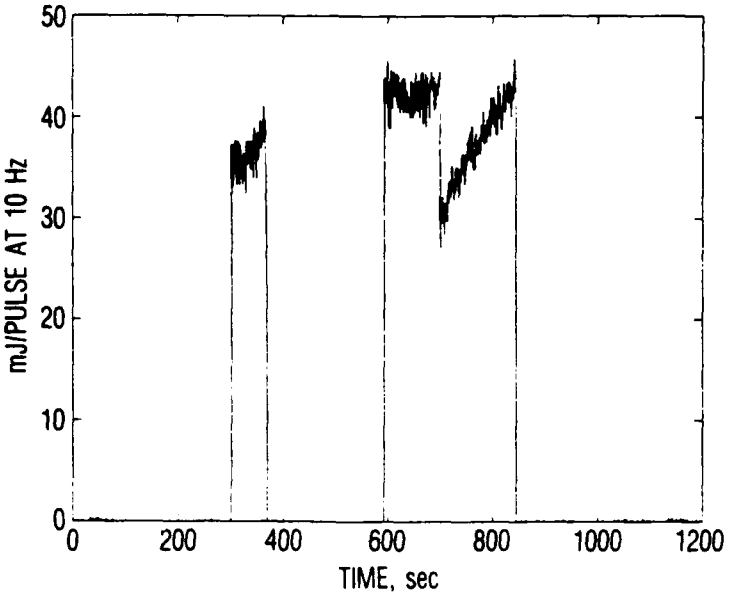

Fig. 8. Photolysis laser power measurement for quantum yield experiment.

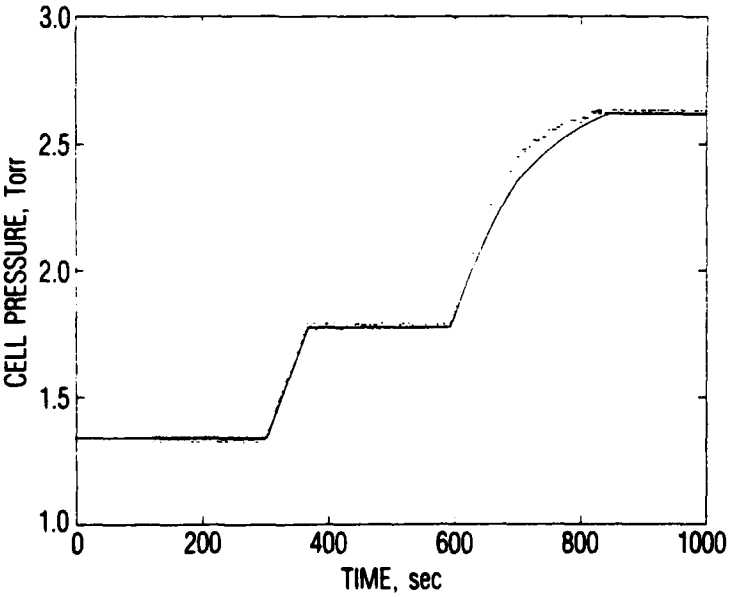

Fig. 9. Measured and calculated cell pressure versus time in quantum yield experiment.

by the Transiac and stored in the computer for signal averaging. Typically, we averaged 400 signal profiles with the ArF photolysis laser operating at 5 Hz. The profiles showed effects of beam steering at long times of 6 to 9 μsec. After recording the signal profile with the laser tuned to the absorption feature, we tuned the dye laser off the absorption feature and repeated the measurement under the same pressure conditions. By subtracting the two profiles, the effects of beam steering could be mostly eliminated. Figure 10 shows an averaged absorption profile obtained at a partial pressure of 0.79 Torr of XeF_2 in helium at a total pressure of 63.1 Torr. Such profiles were recorded at pressures between 4.5 and 90 Torr and were fit with exponential decay curves to obtain the decay rates. The experimental traces showed a fast instrumental rise time, followed by a slower rise time (due to vibrational relaxation) to a profile that could be well described with an exponential decay rate. The solid curve in Fig. 10 shows such a fit to the experimental trace. The decay rates for both helium and neon diluent are plotted in Fig. 11 versus total pressure in the flowtube. The slope of the data gives a removal rate coefficient of $2.0 \pm 0.2 \times 10^4$ $(\text{sec-Torr})^{-1}$ or 6.2×10^{-13} cc/ molecule-sec.

The removal rate of $XeF(X,v=0)$ by collisions with XeF_2 is given by the intercept of the data in Fig. 11. We obtain a rate coefficient of 5.1×10^5 $(\text{sec-Torr})^{-1}$ or 1.6×10^{-11} cc/molecule-sec by dividing the intercept, 0.38×10^6 sec^{-1}, by 0.75 Torr, the partial pressure of XeF_2. This is larger by a factor of about 25 than the removal rate coefficient for helium. This should only be considered an approximate value. At our typical operating conditions, some of the XeF_2 is dissociated by the photolysis laser so that the steady state density is less than the nominal density before the laser is started. By the same token, any xenon and F_2 present under steady state conditions will also contribute to the removal rate at the intercept. However, they should be small contributions relative to the XeF_2.

Decay rates were also measured for XeF(X,v=0) in argon and are plotted in Fig. 12 versus pressure. The argon data have a slope of $2.5 \pm 0.3 \times 10^4$ $(\text{sec-Torr})^{-1}$ or 7.5×10^{-13} cc/molecule-sec, which is about 25% steeper than the data for helium and neon. The intercept of the data has about the same value as the intercept obtained with the helium and neon.

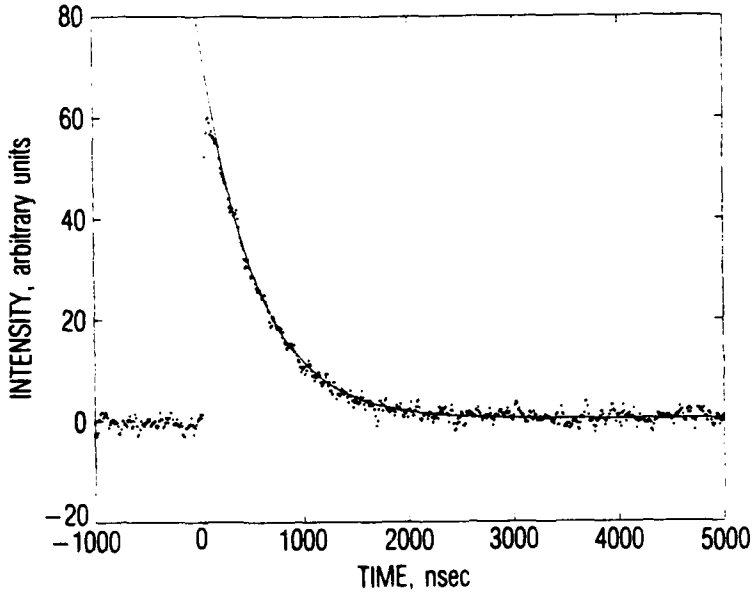

Fig. 10. Time history of XeF(X,v=0) for 0.79 Torr of XeF_2 and 63.1 Torr total pressure of helium. Temperature = 23°C.

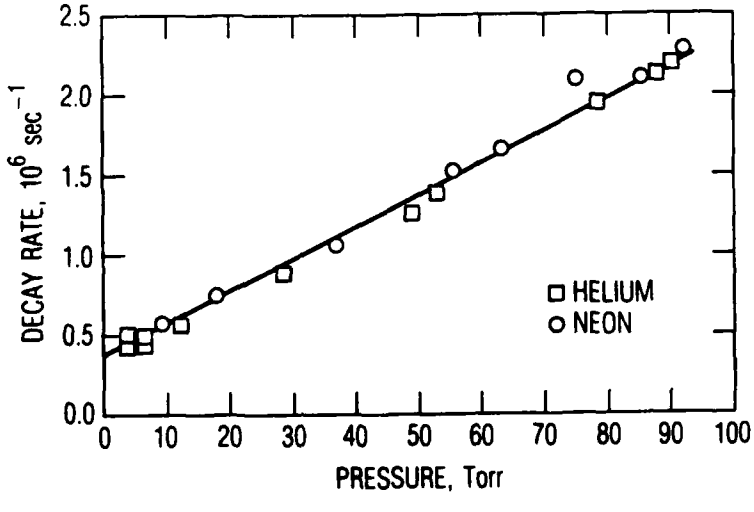

Fig. 11. Decay rates of XeF(X,v=0) versus pressure of helium (squares) and neon (circles). Partial pressures of XeF_2 = 0.72 ± 0.05 Torr. Temperature = 23°C.

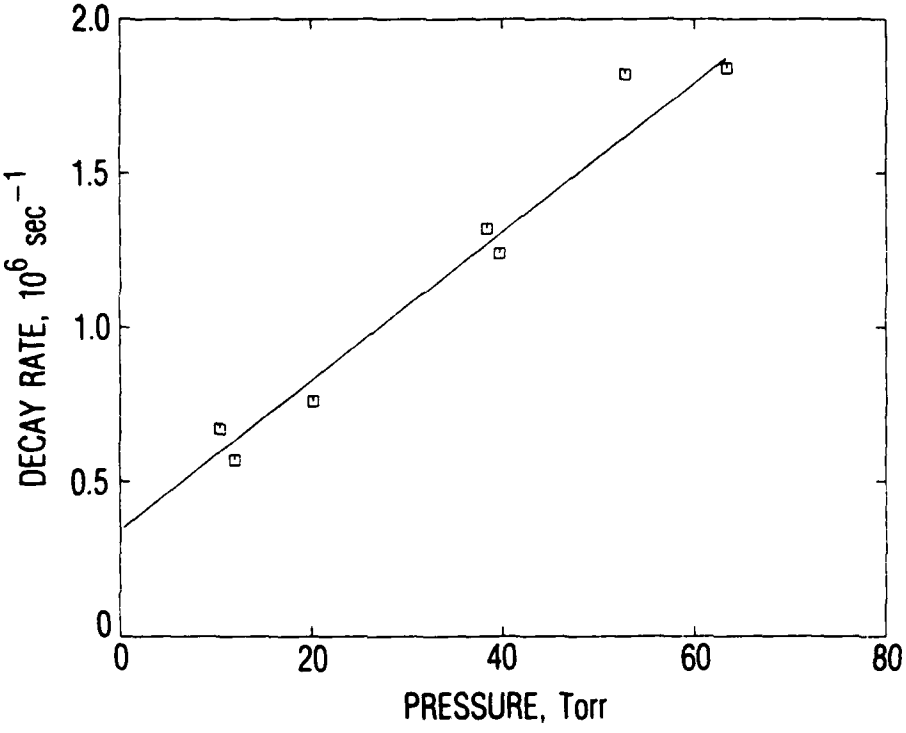

Fig. 12. Decay rates of XeF(X,v=0) versus pressure of argon. Partial pressures of XeF_2 = 0.72 ± 0.05 Torr. Temperature = 23°C.

The photolysis of XeF_2 can produce XeF in the B state, as well as in the ground electronic level. However, the XeF in the B state radiates to the ground electronic state with a 14-nsec lifetime so that within a few tens of nanoseconds there is a "prompt" vibrational distribution produced in the ground electronic state. In Fig. 13 a trace for XeF(X,v=0) at a lower total pressure than that in Fig. 10 shows a prompt population at t = 0, a fast rise to a maximum, and then a slow decay. The rise time is due to vibrational energy transfer between the v = 0 vibrational level and the other vibrational levels. The profiles for XeF(X,v=0) shown by Fulghum et al.[3,4] do not show much, if any, initial population but only a rise time due to vibrational relaxation. Although they used an ArF laser just as we did, our results differ in the observed "prompt" population of XeF(X,v=0).

A set of profiles was measured at total pressures between about 4 and 29 Torr at a partial pressure of 0.25 Torr of XeF_2. The profiles were fit with two exponential terms to determine the exponential rise time. The inverse of these rise times, or rise rates, are plotted in Fig. 14 for helium and neon diluent. Although there is some scatter in the data, there is no substantial difference in the data for the two gases. The slope of Fig. 14 gives a rate coefficient of $0.36 \pm 0.07 \times 10^6$ $(\text{sec-Torr})^{-1}$ or 1.1×10^{-11} cc/molecule-sec. The data have an intercept of $1.8 \pm 0.3 \times 10^6$ sec^{-1}, which may be the vibrational relaxation due to collisions with XeF_2. Based on a partial pressure of 0.25 Torr of XeF_2, this intercept gives a rate coefficient of $7.7 \pm 1 \times 10^6$ $(\text{sec-Torr})^{-1}$ or 2.2×10^{-10} cc/molecule-sec.

D. MEASUREMENTS OF XeF(X,v=1) REMOVAL RATES

We chose an absorption feature in the 1 → 1 band at a nominal wavelength of 345.510 nm for measurements of the removal rates of XeF(X,v=1). Decay rates for XeF(X,v=1) in neon are plotted in Fig. 15 and have a slope of $2.1 \pm 0.2 \times 10^4$ $(\text{sec-Torr})^{-1}$ or 6.5×10^{-13} cc/molecule-sec. Decay rates for XeF(X,v=1) in helium plotted in Fig. 16 have almost the same slope of $2.0 \pm 0.2 \times 10^4$ $(\text{sec-Torr})^{-1}$ or 6.2×10^{-13} cc/molecule-sec. However, the slope of the decay rates in argon shown in the same figure are faster by about 25% than the rates for helium and neon collisions. This is faster in about the same proportion as we observed for XeF(X,v=0) removal rates.

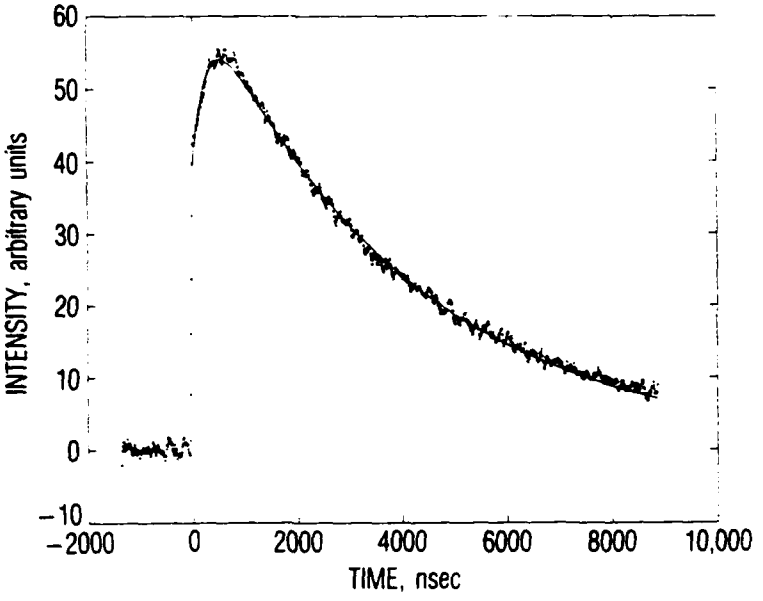

Fig. 13. Time history of XeF(X,v=0) for 0.25 Torr of XeF_2 and 4.47 Torr total pressure of helium. Temperature = 22°C.

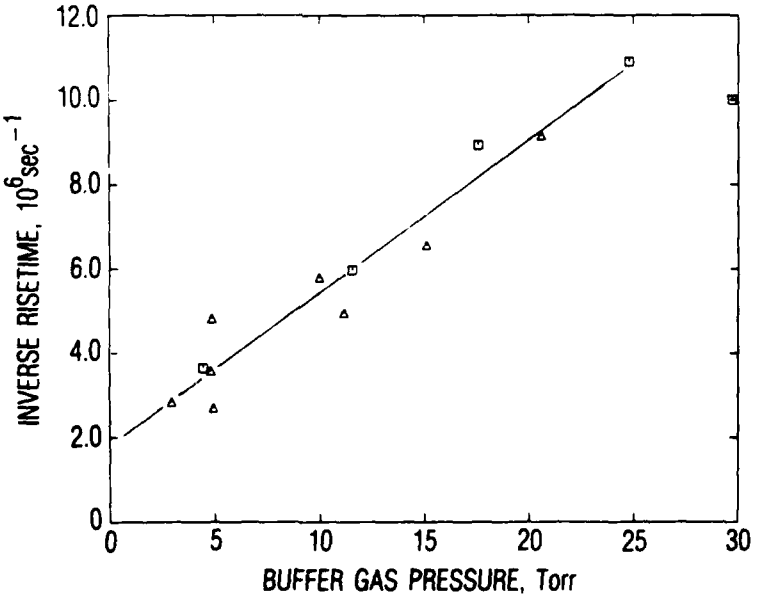

Fig. 14. Inverse rise times of XeF(X,v=0) versus pressure of helium (squares) and neon (triangles). Partial pressures of XeF_2 = 0.25 ± 0.03 Torr. Temperature = 22°C.

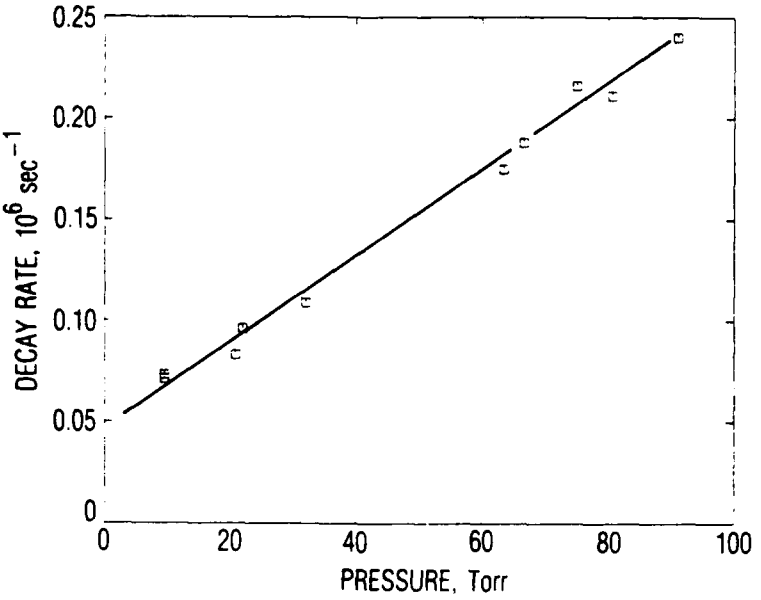

Fig. 15. Decay rates of XeF(X,v=1) versus pressure of neon. Partial pressures of XeF_2 = 1.0 ± 0.05 Torr. Temperature = 26°C.

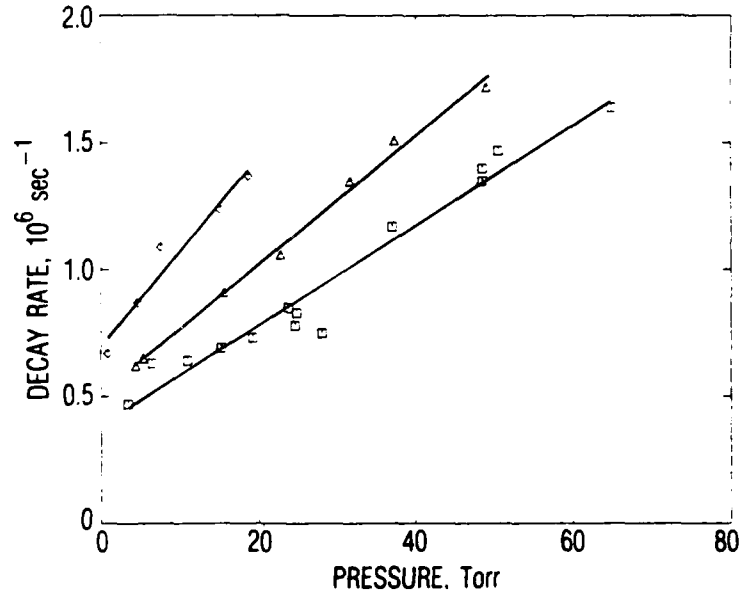

Fig. 16. Decay rates of XeF(X,v=1) versus pressure of helium (squares) and argon (triangles). Decay rates of XeF(X,v=2) versus pressure of argon (diamonds). Partial pressures of XeF_2 = 0.85 ± 0.15 Torr. Temperature = 25 ± 1°C.

E. MEASUREMENTS OF XeF(X,v=2) REMOVAL RATES BY ARGON

We used an absorption feature in the 2 → 2 band at a nominal wavelength of 344.186 nm for measurements of the removal rates of XeF(X,v=2). Decay rates for XeF(X,v=2) have been measured only for argon at pressures between 2 and 18 Torr. These data must be considered preliminary, but they have a slope of $3.7 \pm 0.6 \times 10^4$ $(\text{sec-Torr})^{-1}$ or 1.1×10^{-12} cc/molecule-sec. This is 45% faster than the rate for XeF(X,v=1) removal by argon.

F. EFFECT OF TEMPERATURE ON THE REMOVAL RATES

We have measured rates of XeF(X,v=0) removal by helium and neon at elevated temperatures. The data for helium shown in Fig. 17 indicate removal rates of $2.7 \pm 0.4 \times 10^4$ $(\text{sec-Torr})^{-1}$ or 9.1×10^{-13} cc/molecule-sec at 51°C and $3.5 \pm 0.3 \times 10^4$ $(\text{sec-Torr})^{-1}$ or 1.30×10^{-12} cc/molecule-sec at 85°C. The removal rates for XeF(X,v=0) in neon shown in Fig. 18 indicate rate coefficients of $3.1 \pm 0.3 \times 10^4$ $(\text{sec-Torr})^{-1}$ or 1.09×10^{-12} cc/molecule-sec at 65°C and $4.2 \pm 0.4 \times 10^4$ $(\text{sec-Torr})^{-1}$ or 1.60×10^{-12} cc/molecule-sec at 95°C. These rates are faster than the removal rate of $2.0 \pm 0.2 \times 10^4$ $(\text{sec-Torr})^{-1}$ or 6.2×10^{-13} cc/molecule-sec which we obtained at 23°C (room temperature).

The neon data at 65°C and 95°C were obtained at XeF_2 partial pressures of 0.5 Torr. The rise rates of the absorption traces were determined and are plotted in Fig. 19 versus total pressure. Despite scatter in the data, the slopes can be described with rate coefficients of $2.7 \pm 0.5 \times 10^5$ $(\text{sec-Torr})^{-1}$ and $3.0 \pm 0.7 \times 10^5$ $(\text{sec-Torr})^{-1}$ for the 65°C and 95°C data in neon, respectively. The rate coefficients of 1.1×10^{-11}, 0.95×10^{-11}, and 1.2×10^{-11} cc/molecule-sec at 23, 65 and 95°C show no strong dependence on temperature within the scatter of the data.

The rate coefficients extracted from the intercepts at elevated temperatures of 51 and 85°C are a factor of 2 larger than the room temperature value.

In addition to removing XeF(X), the XeF_2 serves to relax (or mix) the vibrational levels of XeF(X). Fulghum used a "mixing" rate of 2.5×10^6 $(\text{sec-Torr})^{-1}$ to analyze his data. We obtain the larger value of 7.0×10^6 $(\text{sec-Torr})^{-1}$ by extrapolating the inverse rise times of XeF(X,v=0) shown in Fig. 14 to 0.25 Torr, the partial pressure of XeF_2.

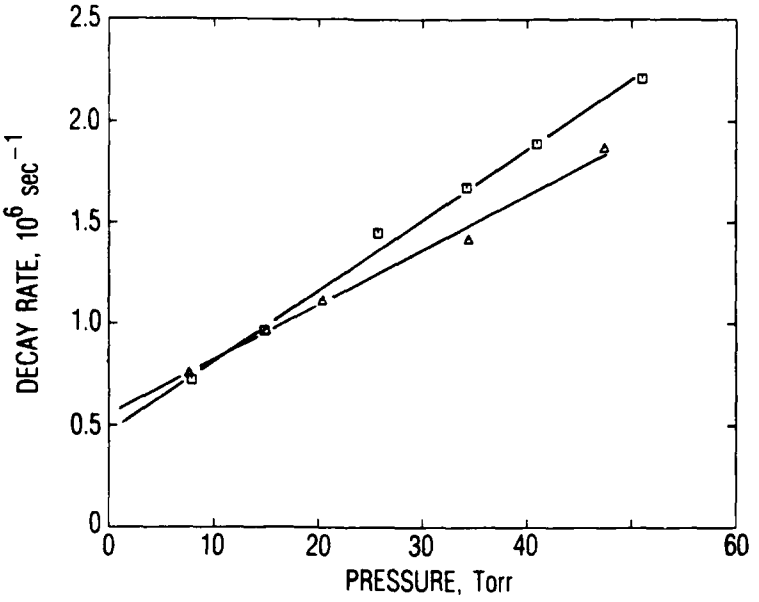

Fig. 17. Decay rates of XeF(X,v=0) versus pressure of helium at elevated temperatures of 51 ± 2°C (triangles) and 85 ± 2°C (squares). Partial pressures of XeF_2 = 0.50 ± 0.05 Torr.

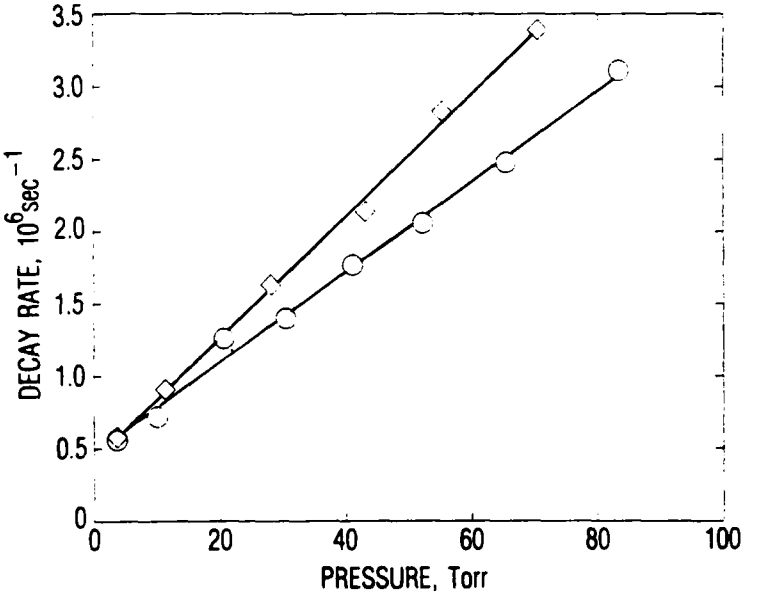

Fig. 18. Decay rates of XeF(X,v=0) versus pressure of neon at elevated temperatures of 65 ± 2°C (circles) and 95 ± 2°C (diamonds). Partial pressures of XeF_2 = 0.50 ± 0.05 Torr.

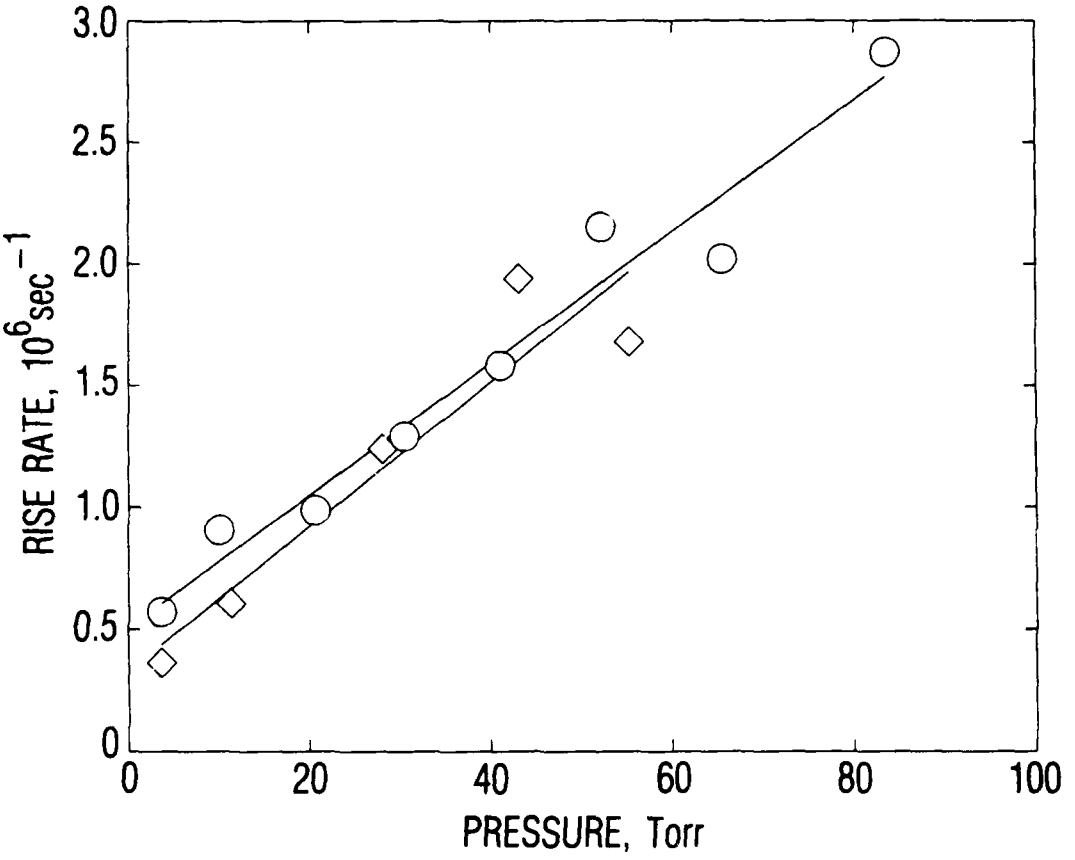

Fig. 19. Rise rates of XeF(X,v=0) versus pressure of neon at elevated temperatures of 65 ± 2°C (circles) and 95 ± 2°C (diamonds). Partial pressures of XeF_2 = 0.50 ± 0.05 Torr.

G. MEASUREMENTS OF XeF(X) REMOVAL BY XeF_2

The rate coefficients for XeF(X,v) removal by XeF_2 can be estimated from the intercepts of Figs. 11, 12, and 15 through 18 and the partial pressures of XeF_2. These data are summarized in Table 1 and indicate a value of 5.0×10^5 $(sec\text{-}Torr)^{-1}$ for the removal rate coefficients for both v = 0 and v = 1 at room temperature. Figure 20 shows the total removal rates obtained at 24°C for v = 1 at several partial pressures of XeF_2 diluted with helium; the total pressure was maintained at 3.4 ± 0.15 Torr to reduce any effects of diffusion. The intercept is the removal rate due to the helium diluent. The slope, 4.5×10^5 $(sec\text{-}Torr)^{-1}$, represents the difference between the removal rate coefficients for XeF_2 and helium. Therefore, the XeF_2 rate coefficient is 4.7×10^5 $(sec\text{-}Torr)^{-1}$, in good agreement with the value deduced above from the intercepts of the several figures. Fulghum et al.[4] reduced their data using a rate of 2.5×10^5 sec^{-1} for the removal of XeF(X,v=1) by 0.6 Torr of XeF_2 or a rate coefficient of 4.2×10^5 $(sec\text{-}Torr)^{-1}$. They used a somewhat larger value of 7×10^5 $(sec\text{-}Torr)^{-1}$ for the rate coefficient for removal of XeF(X,v=0) by XeF_2.

Table 1. XeF(X,v) Removal by XeF_2

Vibrational level, v	Intercept, 10^6 sec^{-1}	XeF_2, Torr	Rate coefficient $(sec\text{-}Torr)^{-1}$	Figure
0	0.38	0.75	0.51×10^6	11
0	0.35	0.75	0.47×10^6	12
1	0.46	0.94	0.49×10^6	15
1	0.50	0.75	0.66×10^6	16, argon
1	0.40	0.85	0.47×10^6	16, helium
0	0.50	0.50	1.00×10^6	17, 85°C
0	0.56	0.50	1.10×10^6	17, 51°C
0	0.47	0.50	0.94×10^6	18, 65°C
0	0.42	0.50	0.84×10^6	18, 95°C

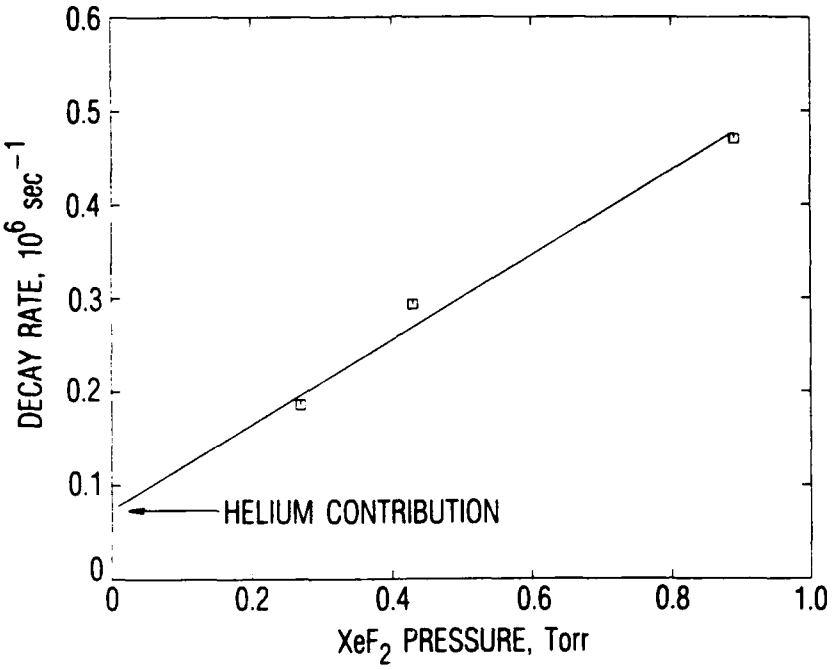

Fig. 20. Decay rates of XeF(X,v=1) in XeF_2 and 3.4 Torr of helium. Helium contribution to decay rate is indicated.

H. OMA MEASUREMENTS OF XeF(B) EMISSION

We have attempted to measure the B-state emission spectrum with an Optical Multichannel Analyzer (OMA). The spectrum is shown in Fig. 21 for XeF_2 at 21°C. In addition to the banded structure, the spectrum shows an underlying continuum; this may result from transitions from the B state to unbound states above the dissociation limit of the ground state. Figure 22 shows the spectrum with the continuum subtracted, leaving only the banded emission features. Integrations of the banded spectrum and the underlying continuum indicate that 10.5% of the B-state emission goes to the bound levels of the ground electronic state and 89.5% goes to the unbound levels. This is a rather large fraction that appears to bypass the XeF ground state.

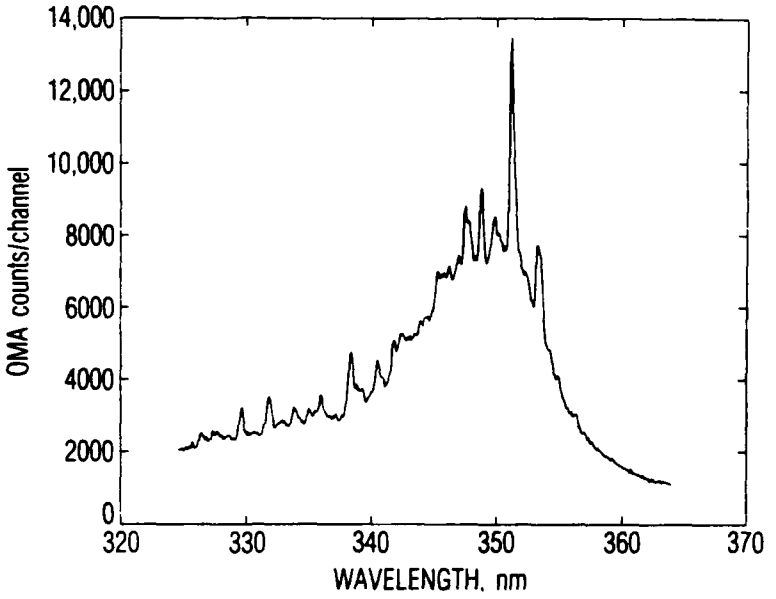

Fig. 21. XeF(B) emission spectrum from the photolysis of XeF_2 at 193 nm.

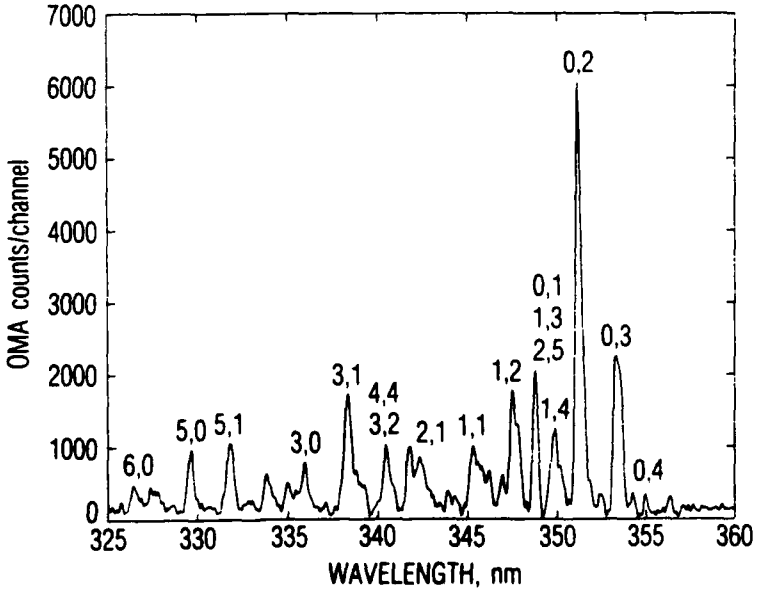

Fig. 22. The XeF(B) emission spectrum of Fig. 21 with the underlying continuum subtracted.

IV. DISCUSSION AND SUMMARY

The present measurements listed in Table 2 show the decay rates of XeF(X,v=0) and XeF(X,v=1) in helium and neon to be the same within the experimental uncertainty. This agrees with the results of Fulghum et al.[3,4] although we find the removal rate coefficient at room temperature, $2.0 \pm 0.2 \times 10^4$ $(\text{sec-Torr})^{-1}$, to be about 50% faster than their reported value of $1.4 \pm 0.4 \times 10^4$ $(\text{sec-Torr})^{-1}$. Our rate coefficient for the removal of v = 0 and 1 by argon is faster than our value for helium and neon by 25%. The fast vibrational relaxation of XeF(X,v) by the diluent gas brings the initial populations into a coupled distribution over the vibrational manifold so that it decays with a single decay rate. At least, this appears to be the case for v = 0 and 1. This coupling may break down at the higher vibrational levels where the state-to-state dissociation rates can be expected to be much faster. Some evidence of this may be showing up in the preliminary rate for XeF(X,v=2) decay in argon which appears to be faster than the rates for v = 0

Table 2. XeF(X,v) Removal by Argon, Helium, and Neon

Vibrational level, v	Temp, °C	Rate coefficient $(\text{sec-Torr})^{-1}$	Collision partner
0	23	$2.0 \pm 0.2 \times 10^4$	helium, neon
0	23	$2.5 \pm 0.3 \times 10^4$	argon
1	26	$2.0 \pm 0.2 \times 10^4$	helium
1	26	$2.1 \pm 0.2 \times 10^4$	neon
1	25	$2.5 \pm 0.3 \times 10^4$	argon
2	25	$3.7 \pm 0.6 \times 10^4$	argon
0	51	$2.7 \pm 0.4 \times 10^4$	helium
0	85	$3.5 \pm 0.3 \times 10^4$	helium
0	65	$3.1 \pm 0.3 \times 10^4$	neon
0	95	$4.2 \pm 0.4 \times 10^4$	neon

and 1 in argon. This coupling makes it necessary to perform modeling calculations in order to compare experimental data with theoretical state-to-state rate coefficient calculations such as those by Wilkins.[5]

The decay rate coefficients for v = 0 increase with temperature as shown in Fig. 23. Dissociation rate coefficients are typically described by equations of the form $A \times T^n \times \exp(-E/RT)$. A least squares fit to the decay rate coefficients in Fig. 23 gives E = 1200 cm^{-1} for n set equal to -1. This is within 150 cm^{-1} of the spectroscopic value of the dissociation energy, 1063 cm^{-1}. Because of the limited temperature range, these values of the parameters are not unique, and a fit can also be made with n = 0 and E = 962 cm^{-1}.

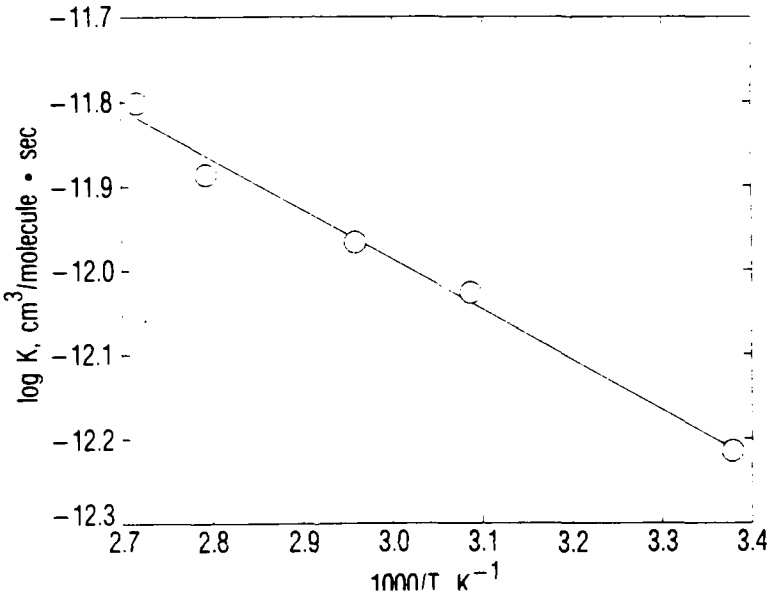

Fig. 23. Decay rate coefficients for XeF(X,v=0) in helium and neon versus 1000/T.

We have calculated the rate coefficient for the recombination of Xe and F atoms from the dissociation rate coefficient and the equilibrium constant and obtained a value of 4.5×10^{-33} (cc/molecule)^2/sec or $10^{9.2}$ (liter/mole)^2/sec for the recombination rate coefficient at 296 K. Benson[12] tabulated atom recombination rate coefficients and noted that they all seem to lie near $10^{9.5\pm0.5}$ (liter/mole)^2/sec at 300 K. Therefore, the present measurements seem reasonable even though the small bond energy of XeF distinguishes it from most other molecules. The recombination rate coefficient is essentially constant within our limited range of temperatures, although the recombination rate coefficients tabulated by Benson tend to have a T^{-1} dependence.

A major difference between the present results and those of Fulghum et al. is the value of the v = 0 to 1 vibrational excitation rate coefficient. Our value of $3.6 \pm 0.7 \times 10^5$ (sec-Torr)$^{-1}$ or 1.1×10^{-11} cc/molecule-sec for both helium and neon compares with the slower rate of $4.81 \pm 1.49 \times 10^4$ (sec-Torr)$^{-1}$ or 1.5×10^{-12} cc/molecule-sec reported by Fulghum et al.[3] This fast vibrational relaxation rate is expected, since the energy spacing between v = 0 and v = 1 is only about 204 cm^{-1}. At 300 K, the collision partners have an average collision energy, RT, of 205 cm^{-1}. Because the rate coefficients are so fast, it is not surprising that they show no dependence on temperature within the scatter of our data and in the limited temperature range. Fulghum et al.[3] pointed out that the rise rate should be interpreted as a weighted average of the VT rates for the several vibrational levels. In addition to the faster rates, we see a significant population in the v = 0 level, whereas Fulghum's v = 0 profiles did not show such initial population. Since we both used an ArF laser for the photolysis of XeF_2, we should have observed the same initial populations in v = 0.

The state-to-state rate coefficients for vibrational relaxation are needed for laser modeling. Fulghum et al.[4] used a vibrational relaxation model to generate these values. This same model could be used with the present data also. Wilkins[5] has recently calculated vibrational relaxation rates which are faster than those deduced by Fulghum. Wilkins calculated 7.4×10^{-12} cc/molecule-sec for the v = 1 to 0 relaxation by neon and 1.0×10^{-11} cc/molecule-sec for the v = 1 to 0 relaxation by helium. The rate

coefficients of Wilkins[5] may be in fair agreement with the present vibrational relaxation data. A detailed kinetic calculation for the several vibrational levels will be required to determine how well they predict the present results.

The present measurements of the XeF_2 absorption at 193 and 253 nm appear to resolve the discrepancy in the absorption measurements plotted in Fig. 1 of Ref. 10. Adjusting the data in that figure to match our values at these two wavelengths brings the two sets of measured absorption coefficients into agreement in their overlapping wavelength interval.

Black et al.[10] reported the B-state quantum yield for the photolysis of XeF_2 to be 0.9 (+0.1, -0.2) between 146 and 172 nm. In the present studies we determined that the absorption of a 193-nm photon leads to the removal of one molecule of XeF_2. We cannot state what fraction of the photolysis produces an XeF molecule in the B state; however, this channel is possible up to the energetic threshold[1] of 204 nm. Therefore, a photon at 193 nm has energy sufficient to produce XeF(B) with 2790 cm^{-1} of vibrational/rotational energy. This energy corresponds to a vibrational level of about v = 9 in the B state. We have recorded the emission from the B state with an Optical Multichannel Analyzer (OMA). In addition to the banded structure, the spectrum shows an underlying continuum which may result from transitions from the B state to unbounded states above the dissociation limit of the ground state. Integrations of the banded spectrum and the underlying continuum indicate that 10.5% of the B-state emission goes to the bound levels of the ground electronic state and 89.5% goes to the unbound levels. This is a rather large fraction of the B-state emission that appears to bypass the XeF ground state.

We can calculate the expected absorption on a vibrational/rotational feature of XeF(X,v=0) using rough estimates of the populations in the vibrational/rotational levels. The absorption can be written as follows:

$$\ln I_o/I = \sigma_{350} \times 1/8 \times 1/4 \times 1/50 \times P \times \left(1-\exp(-\sigma_{193} \times \ell \times [XeF_2])\right)$$

where σ_{350} is the absorption cross-section at the peak of a Doppler-broadened profile, P = 1.2×10^{17} photons/cm^2, ℓ = 75 cm, σ_{193} is the cross section for absorption by XeF_2 at 193 nm, 1/8 is the fraction of XeF(X) in v = 0, 1/4 is the isotopic fraction, and 1/50 is the rotational partition fraction. The absorption cross-section at 350 nm was calculated on the basis of the lifetime of the B state. When we substitute in the values of these quantities, we obtain an absorption coefficient of 7 which is much larger than the observed quantities of 0.1 to 0.2. Although the OMA measurements indicated only 10% of the B state decays to the bound ground state, the quantum yield of the B state may in fact be low. The explanation that the absorption of a photon by XeF_2 leads directly to the dissociation products of Xe and F atoms seems unlikely.

In addition to removing XeF(X), the XeF_2 serves to relax (or mix) the vibrational levels. Fulghum et al.[4] used a "mixing" rate of 2.5×10^6 (sec-Torr)$^{-1}$ to analyze their data, whereas we obtained the somewhat larger value of 7×10^6 (sec-Torr)$^{-1}$. These are large rate coefficients since 2.5×10^6 (sec-Torr)$^{-1}$ is approximately a gas kinetic rate coefficient for a collision cross section of 3 Å. Fulghum et al.[4] suggested that the fast vibrational rate coefficient was the result of the near resonance between the bending mode of XeF_2 (212 cm^{-1}) and the 0 → 1 vibrational transition of XeF (204 ± 4 cm^{-1}).

In summary, the present experiments have demonstrated that XeF(X,v) can be produced in sufficient quantities that absorption measurements can be used to determine their disappearance rates. We plan to use this technique and extend the measurements to the higher vibrational levels of XeF(X) on which the XeF laser transitions terminate. The present results confirm the removal rates of XeF measured by Fulghum et al.[2,3,4], although our measured values are about 50% faster. However, we measure a much faster vibrational relaxation rate. This faster rate should be important in evaluating the theoretical performance of the XeF laser and the effects of "bottlenecking" on the lower levels of the laser transitions.

REFERENCES

1. P. Tellinghuisen, J. Tellinghuisen, J. A. Coxon, J. E. Velazco, and D. W. Setser, J. Chem. Phys. 68, 5187 (1978).

2. S. F. Fulghum, M. S. Feld, and A. Javan, Appl. Phys. Lett. 33, 926 (1978).

3. S. F. Fulghum, M. S. Feld, and A. Javan, Appl. Phys. Lett. 35, 247 (1979).

4. S. F. Fulghum, M. S. Feld, and A. Javan, IEEE J. Quantum Electron. 16, 815 (1980).

5. R. L. Wilkins, Theoretical Calculations of XeF Ground State Kinetics, TR-0086A(2061)-1, The Aerospace Corporation, El Segundo, Calif. (1 March 1988).

6. J. G. Eden and R. W. Waynant, Opt. Lett. 2, 13 (1978).

7. H. Helm, L. E. Jusinski, D. C. Lorents, and D. L. Huestis, J. Chem. Phys. 5, 1796 (1984).

8. F. Schreiner, G. N. McDonald, and C. L. Cherick, J. Phys. Chem. 72, 1162 (1968).

9. J. B. Koffend, XeF Spectrum Simulation, ATM 85(5930-01)-2, The Aerospace Corporation, El Segundo, Calif. (25 April 1985).

10. G. Black, R. L. Sharpless, D. C. Lorents, D. L Huestis, et al., J. Chem. Phys. 75, 4840 (1981).

11. J. Jortner, E. G. Wilson, and S. A. Rice, in Noble-Gas Compounds, ed. H. H. Hyman, University of Chicago, Chicago (1963).

12. S. W. Benson, Thermochemical Kinetics, John Wiley & Sons, New York, p. 179 (1976).

LABORATORY OPERATIONS

The Aerospace Corporation functions as an "architect-engineer" for national security projects, specializing in advanced military space systems. Providing research support, the corporation's Laboratory Operations conducts experimental and theoretical investigations that focus on the application of scientific and technical advances to such systems. Vital to the success of these investigations is the technical staff's wide-ranging expertise and its ability to stay current with new developments. This expertise is enhanced by a research program aimed at dealing with the many problems associated with rapidly evolving space systems. Contributing their capabilities to the research effort are these individual laboratories:

Aerophysics Laboratory: Launch vehicle and reentry fluid mechanics, heat transfer and flight dynamics; chemical and electric propulsion, propellant chemistry, chemical dynamics, environmental chemistry, trace detection; spacecraft structural mechanics, contamination, thermal and structural control; high temperature thermomechanics, gas kinetics and radiation; cw and pulsed chemical and excimer laser development including chemical kinetics, spectroscopy, optical resonators, beam control, atmospheric propagation, laser effects and countermeasures.

Chemistry and Physics Laboratory: Atmospheric chemical reactions, atmospheric optics, light scattering, state-specific chemical reactions and radiative signatures of missile plumes, sensor out-of-field-of-view rejection, applied laser spectroscopy, laser chemistry, laser optoelectronics, solar cell physics, battery electrochemistry, space vacuum and radiation effects on materials, lubrication and surface phenomena, thermionic emission, photosensitive materials and detectors, atomic frequency standards, and environmental chemistry.

Computer Science Laboratory: Program verification, program translation, performance-sensitive system design, distributed architectures for spaceborne computers, fault-tolerant computer systems, artificial intelligence, microelectronics applications, communication protocols, and computer security.

Electronics Research Laboratory: Microelectronics, solid-state device physics, compound semiconductors, radiation hardening; electro-optics, quantum electronics, solid-state lasers, optical propagation and communications; microwave semiconductor devices, microwave/millimeter wave measurements, diagnostics and radiometry, microwave/millimeter wave thermionic devices; atomic time and frequency standards; antennas, rf systems, electromagnetic propagation phenomena, space communication systems.

Materials Sciences Laboratory: Development of new materials: metals, alloys, ceramics, polymers and their composites, and new forms of carbon; nondestructive evaluation, component failure analysis and reliability; fracture mechanics and stress corrosion; analysis and evaluation of materials at cryogenic and elevated temperatures as well as in space and enemy-induced environments.

Space Sciences Laboratory: Magnetospheric, auroral and cosmic ray physics, wave-particle interactions, magnetospheric plasma waves; atmospheric and ionospheric physics, density and composition of the upper atmosphere, remote sensing using atmospheric radiation; solar physics, infrared astronomy, infrared signature analysis; effects of solar activity, magnetic storms and nuclear explosions on the earth's atmosphere, ionosphere and magnetosphere; effects of electromagnetic and particulate radiations on space systems; space instrumentation.

END
DATED
FILM
8-88
DTIC